Journal of Materials Science: Materials in Electronics, Volume 30, Issue 24, December 2019, pp. 21229–21239
DOI:10.1007/s10854-019-02496-2

Construction of porous hierarchical $NiCo_2S_4$ toward high rate performance supercapacitor

Zhao F[a,b], Huang W[c], Sial, M.A.Z.G.[a,b], Xie D.[a], Wu H.[a], Zhang Q.[d], Zou J.[a] & Zeng, X[a,b]

[a]Shenzhen Key Laboratory of Special Functional Materials and Shenzhen Engineering Laboratory for Advance Technology of Ceramics, College of Materials Science and Engineering, Shenzhen University, Shenzhen, 518060, China
[b]Key Laboratory of Optoelectronic Devices and Systems of Ministry of Education and Guangdong Province, College of Optoelectronic Engineering, Shenzhen University, Shenzhen, 518060, China
[c]College of Materials Science and Engineering, Sichuan University, Chengdu, 610065, China
dDepartment of Manufacturing and Materials, Cranfield University, Cranfield, Bedfordshire, MK43 0AL, United Kingdom

Abstract

Developing high-performance supercapacitors is an effective way to meet the ever-increasing energy storage demand for emerging devices, but the inferior rate performance, especially for battery-type supercapacitors, limits their large-scale utilization. Herein, the porous hierarchical nickel cobalt sulfide ($NiCo_2S_4$) was constructed by a novel strategy that the synthesized nickel cobalt oxide nanosheets as chemical template by hydrothermal method. Furthermore, the backbone of nickel cobalt oxide nanosheets converted to $NiCo_2S_4$, which extremely enhances entire conductivity and keeps playing the role of matrix support to buffer the volume variation. Benefiting from high specific area (79.9 m^2 g^{-1}), suitable nanopores for KOH electrolyte, and multiple Co/Ni valence, the hierarchical $NiCo_2S_4$ electrode delivers a high capacity of 1035.1 F g^{-1} at a current density of 1 A g^{-1}, and an ultrahigh rate performance of 80.9% capacitance retention at 20 A g^{-1}. In addition, the assembled asymmetric supercapacitor device (activated carbon as negative electrode) could achieve the maximum capacity of 102.4 F g^{-1} at 5 mV s^{-1} and well maintain at 80.5 F g^{-1} at 50 mV s^{-1}. The maximum energy density of 35.4 Wh kg^{-1} can be obtained at a power density of 0.4 kW kg^{-1}. These results indicate that this hierarchical $NiCo_2S_4$ could be served as high rate performance electrode materials for advanced supercapacitors.

Keywords: hierarchical structure, $NiCo_2S_4$, high specific area, supercapacitors

1. Introduction

In the 21st century, environmental pollution and energy crisis have promoted to accelerate the sustainable development of green economy/energy. Therefore, the evolution of clean energy (such as solar, wind, and nuclear energy) is imperative [1].

Meanwhile, new energy storage devices need to be developed to adapt the renewable resources to overcome future energy anxiety. Among them, supercapacitors (also known as electrochemical capacitors) have drawn a widespread attention owing to their special strength, such as cyclical stability, high power density and fast charge/discharge rate [2]. These merits endow them a broad potential application in electric vehicles, uninterrupted power supplies, smart microgrids and wind turbine pitch field, *etc*. Electrode materials are the vital component of supercapacitors and their capacity governs the whole devices. Development of high-performance supercapacitors electrode materials mainly derives from three kinds of materials, such as conducting polymers, transition metal compounds, and carbonaceous materials. Conductive polymers are cost-effective but yield to capacitance and cycling ability. Carbonaceous materials are superior to cyclic and rate performance, but subject to low capacity and energy density. As for transition metal compounds, they have the unparalleled advantage of high specific capacitance and energy density. Among transition metals, nickel cobalt compounds materials (such as sulfides, oxides[3], hydroxides[4], and nitrides[5]), are regarded as the most potential electrode materials owing to their conductivity, theoretical capacity, redox activity, eco-friendly and vast reserves.

Spinel ternary nickel cobalt sulfides ($NiCo_2S_4$ or $CoNi_2S_4$), as a novel class of nonprecious electrode materials, draw an extensive attention owing to their narrow band gap (E_g = 2.4V) with a high conductivity, 100 times higher than $NiCo_2O_4$ or corresponding single metal sulfides (such as Ni_2S_3, Co_8S_9, CoS) [6, 7]. Due to their superior electrical conductivity, nickel cobalt sulfides are the most researched for supercapacitors, Li ion batteries, Zn-Air batteries, Na ion batteries, solar cells, and fuel cells[8]. However nickel cobalt materials suffer from inferior rate performance and cycle ability (actually, it is a common problem of battery-type materials) as comparable to EDLC, which hinders them from a wide scope of applications. For example, Wu [9]et al synthesized $NiCo_2S_4$ nanosheets exhibiting a high specific capacitance of 744 F g^{-1} at 1 A g^{-1} but suffering from an inferior cycle performance. Similarly, Yu [10] et al fabricated $NiCo_2S_4$ discs with a capacitance of 908 F g^{-1} at 3 A g^{-1} but subjected to poor rate performance of 610 F g^{-1} at 20 A g^{-1}. To address these cycling and rate problems, nanostructured engineering is the most common strategy to overcome these issues, and various nanostructured architectures of $NiCo_2S_4$ (for example, cage, tube, sheet, sphere, wire, and hollow ball) had been constructed and made some improvements [11, 12]. However, nanostructured materials cannot avoid the problem of self-aggregate because of their high surface energy, and the self-aggregation of nanostructured materials decreases specific area and redox sites [13]. Consequently, templates are introduced to improve electrochemical performance. Up till now, $NiCo_2S_4$ growth normally on carbon cloth [12], nickel foam [14], zeolitic imidazole frameworks [15], Polyaniline [16], $Co(OH)_2$ [17], $NiCo_2O_4$ [18], CNTs [19], and graphene [20]. These reported substrates are normally physical templates which could not disappear or dissolve and were kept as the second phase for composites with the growth of $NiCo_2S_4$. Thus, the conductivity of composites is obviously improved because the second phase has a much lower conductivity than $NiCo_2S_4$ (except CNTs and graphene). Consequently, it will be challenging to find a kind of material that can play a template role and eventually

converted to $NiCo_2S_4$.

According to previous literature, $NiCo_2O_4$ is much stable than $NiCo_2S_4$ because of the oxygen saturation, implying the possibility of high cycle stability [18]. Our previous research [21] indicated that $NiCo_xO_y$ nanosheets remains 86.5% of its initial capacity after 4 000 cycles but the capacity is still unsatisfactory. Consequently, it would be promising that the combination of spinel nickel cobalt oxides and sulfides with their strengths of cycle stability and capacitance, respectively. Actually, the combination of $NiCo_2O_4$ and $NiCo_2S_4$ was reported [xx], and the combined materials were normally prepared on nickel foam or carbon cloth substrate and the $NiCo_2O_4$ phase was remained, which struggle to reach excellent electrochemical performance [22, 23]. Specifically, three-dimensional $NiCo_2O_4$/$NiCo_2S_4$ hybrids were deposited on nickel foam and obtained high specific capacitance, but the capacitance retention could just keep 75.4% with 4-fold increase of current density [24]. This implies the absence of $NiCo_2O_4$ increase electrical resistivity of the whole composites and further affects the rate performance. To address these problems, the backbone of $NiCo_xO_y$ nanosheets were firstly constructed and then converted to sulfides, and $NiCo_2S_4$ nanoparticles were grown on them by the same time. Besides, due to the introduction of sheets, the nanoparticles could both avoid agglomerating and achieve high specific area along with rich redox sites. Inspired by above consideration, we focus on exploring a template-free method to prepare hierarchical $NiCo_2S_4$ electrode materials toward high rate energy storage devices.

In this paper, we synthesized $NiCo_2S_4$ powders along with achieving the goal of template converted to $NiCo_2S_4$. Benefiting from the backbone architecture and high specific area, the synthesized $NiCo_2S_4$ exhibits superior electrochemical performance, especially in rate performance. In addition, a hybrid asymmetric supercapacitor (ASC) was successfully assembled and it delivered a high energy density and excellent rate performance.

2. Experimental section

2.1. Materials and synthesis

1.164 g $Co(NO_3)_2{\cdot}6H_2O$, 0.582 g $Ni(NO_3)_2{\cdot}6H_2O$, and 1.207 g hexamethylenetetramine were dissolved into 20 mL ethanol and 50 mL deionized water (donated as DI water). The solution was heated at 120 °C for 2 h under reflux. After cooling, precipitates were washed with DI water and ethanol and then dried in a blast oven at 60 °C. The dried materials were calcined in air atmosphere at 300°C for 2 h to obtain self-assembled $(NiCo_y)_3O_4$ nanosheets.

0.3 g $(Ni_xCo_y)_3O_4$ nanosheets were dispersed in 60 mL DI water under strong ultrasonic treatment. The 60 mL dispersion was then mixed with 20 mL ethanol, 0.582 g $Ni(NO_3)_2{\cdot}6H_2O$, 1.164 g $Co(NO_3)_2{\cdot}6H_2O$, 0.72 g urea, and 0.6 g thioacetamide. Finally, the mixture was transferred to a 100 mL hydrothermal vessel and heated in an oven at 200 °C for 12 h. After naturally cooling, the precipitates were collected and washed by DI water and ethanol several times. Finally, they were dried in a vacuum oven at 60 °C for 12 h and then the $NiCo_2S_4$ powders were obtained.

2.2 Material Characterization

The crystal phases of the samples were characterized by X-ray diffraction (XRD, Miniflex600, Rigaku) by Cu K_α (λ= 0.15418 nm) radiation. The microstructure was directly examined by high resolution transmission electron microscopy (HRTEM, FEI Tecnai G20) furnished with selected area electron diffraction, and field emission scanning electron microscopy (FESEM, Hitachi SU-70). X-ray photoelectron spectroscopy (XPS, Microlab 350) was carried out to measure sample's surface chemical states (Al K_α source). The N_2 adsorption/desorption isotherms and Brunauer-Emmett-Teller (BET) specific surface area of the samples were measured at liquid nitrogen temperature (77 K) by Micromeritics ASAP 2010.

2.3 Electrochemical Characterization

The electrochemical performance of the sample was evaluated via electrochemical workstation (CHI660E, Chenhua). The working electrode was fabricated by following procedure: 80 wt.% active material ($NiCo_2S_4$), 10 wt.% acetylene black, and 80 wt.% polyvinylidene difluoride were mixed in N-methyl pyrrolidone (NMP), coated on nickel foam, and then pressed by 10 MPa. The average mass load of active material on nickel foam is 2 ~ 3 mg. Besides, Hg/HgO, platinum plate (1.5 × 1.5 cm), and 3 M KOH and were used as reference electrode, counter electrode and aqueous electrolyte, respectively. The capacitance of the electrode can be calculated by the following equation:

$$C_m = \frac{I\Delta t}{m\Delta V} \quad (1)$$

Where I (A), Δt (s), m (g), and ΔV (V), represent current, discharge time, mass of active material, and discharge potential window, respectively. A hybrid asymmetric supercapacitor was assembled, where $NiCo_2S_4$ and activated carbon were used as positive and negative electrode, respectively. To balance the positive/negative electrode charge (Q_+=Q_-) during the assembly, the mass of each electrode could be trimmed by the following equations:

$$Q=C_mV \quad (2)$$

$$\frac{m^+}{m^-} = \frac{C_- \times \Delta V_-}{C_+ \times \Delta V_+} \quad (3)$$

In addition, the energy density (E, Wh kg^{-1}) and power density (P, W kg^{-1}) of the ASC devices can be calculated by the following equations (based on the whole weight of active materials of device):

$$E = \frac{CV^2}{2\times3.6} \quad (4)$$

$$P = \frac{3600\times E}{\Delta t} \quad (5)$$

3. Results and discussion

Scheme 1 summarizes the overall synthesis process of hierarchical $NiCo_2S_4$. Briefly, nanosheet structured Ni-Co precursors were prepared by the heated reaction solution under reflux condensation. Water and carbon dioxide will volatilize and escape

from core zone during the calcination process, and the porous and rough nickel cobaltite could be synthesized with the help of gas escape. Then, owing to the introduction of nanosheet matrix, $NiCo_2S_4$ nanoparticles were preferential growing on nanosheets (heterogeneous nuclei factor) and simultaneously sulfurizes nickel cobaltite. Finally, hierarchical $NiCo_2S_4$ was obtained.

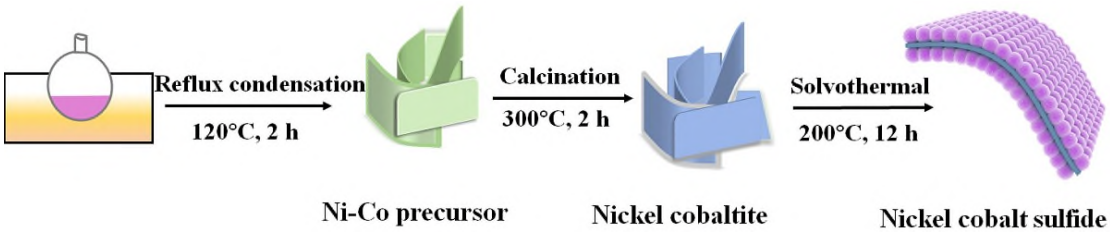

Scheme 1 Synthesis diagram of $NiCo_2S_4$

The samples were firstly analyzed by XRD to confirm their phase and crystallinity, as presented in Figure 1a. The calcined products can be easily indexed to spinel nickel cobaltite $Ni_{1.71}Co_{1.29}$ O_4 (denoted as NCO, JCPDS 40-1191). Then $NiCo_2S_4$ was synthesized on NCO substrate by hydrothermal method. As for nickel cobalt sulfides, it can be found that main diffraction peaks of the pattern can correspond to the lattice planes of (220), (311), (400), (511) and (440) with $NiCo_2S_4$ (JCPDS 20-0782) at 26.54°, 31.48°, 38.14°, 50.44° and 55.14°, respectively. NCO peaks were not observed in the patterns, which could be the displacement of O by S atom because of sulfur addition. From the SEM image of NCO (Figure 1b), the self-assembled structured nanosheets (NCO) can be observed with a length of around 1 μm. Figure 1c and d display the morphology of $NiCo_2S_4$ by SEM with different magnifications. It can be found that $NiCo_2S_4$ is mainly composed of a few micrometers (length direction) of sheets with basal growth of some much smaller nanoparticles with ca. 40 nm in size. The self-assembled nanosheet NCO could be detached after dispersion treatment, and then nanoparticles could anchor on nanosheet, which can be confirmed by the hierarchical $NiCo_2S_4$ (as shown in Figure 1d). This indicates that $NiCo_2S_4$ is composed of the structured $NiCo_2S_4$ nanosheet converted by NCO through sulfidation and new $NiCo_2S_4$ nanoparticles anchored on the surface of nanosheets. The nanosheet structure provides a scaffold support to the growth of particle and avoid agglomeration, which is beneficial to high porosity. Combined with aforementioned XRD analysis, the NCO also acts as a template-free role.

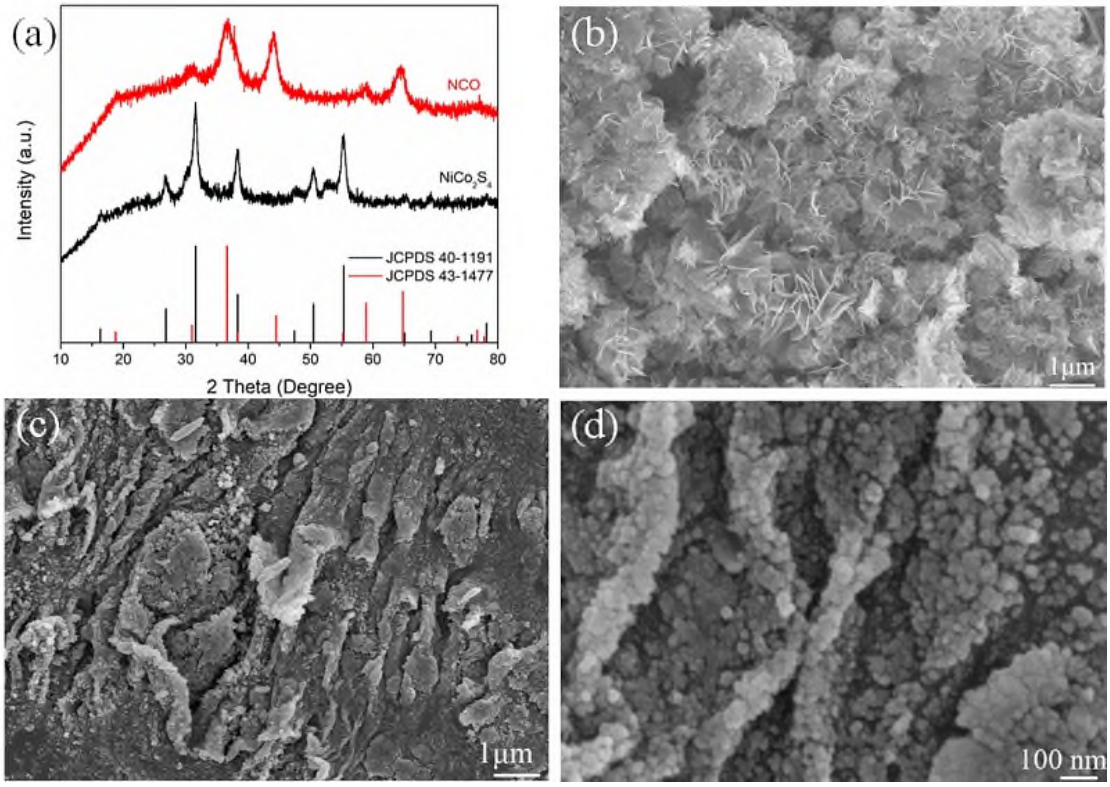

Figure 1 (a) XRD patterns of NCO and $NiCo_2S_4$, (b) SEM images of NCO, (c, d) SEM images $NiCo_2S_4$ with different magnification.

More intrinsic features of the hierarchical $NiCo_2S_4$ were explored by TEM and HRTEM, as presented in Figure 2. Figure 2a indicates that the nanoparticles are closely anchored on the nanosheet. From the HRTEM image (Figure 2b), the well-defined lattice fringes with different grain orientation can be easily recognized that it confirms the polycrystalline and high crystallinity characteristics. Moreover, the lattice interplanar space of 0.33 and 0.28 nm exactly matches the (220) and (311) planes of $NiCo_2S_4$, respectively. According to the selected area electron diffraction (SAED) patterns, a series of diffraction ring-spots could be observed, which confirmed polycrystalline. These ring-spots can be indexed to (220), (311), (400), (511), and (440) planes, which is in good agreement to the XRD analysis and reinforces the composition of $NiCo_2S_4$.

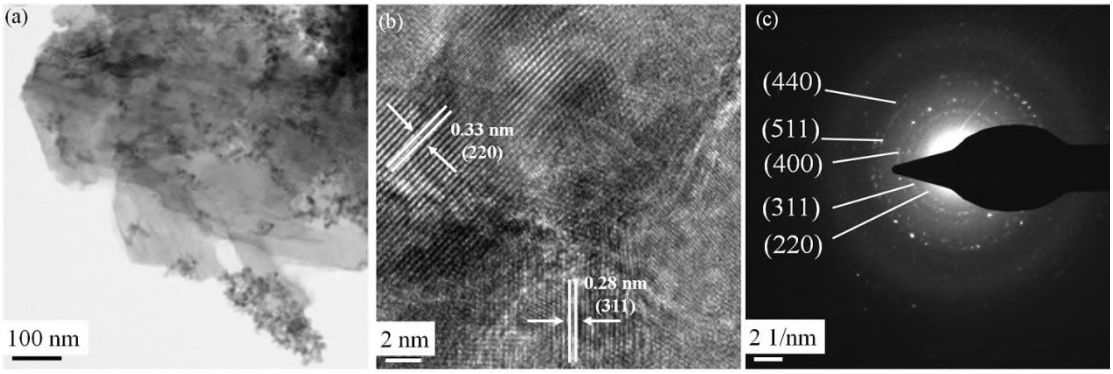

Figure 2 (a) TEM image, (b) HRTEM, and (c) SAED pattern of $NiCo_2S_4$.

The surface elemental valence composition and bond states were probed by XPS. The overall spectrum of $NiCo_2S_4$ is presented in Figure 3, which manifests that the

sample is composed of Ni, Co, and S elements. The Ni 2p core-level spectrum is shown in Figure 3b, where two spin-orbit doublets ($2p_{3/2}$ and $2p_{1/2}$) and two shake-up satellites (marked as "Sat.") are observed. The binding energy of Ni 2p (Figure 3b) centered at 853.1 and 870.5 eV corresponds to Ni^{2+}, and peaks at 856.2 and 874.1 eV can be ascribed to Ni^{3+}. Similarly, the Co 2p spectrum (Figure 3c) can also be divided $2p_{3/2}$ and $2p_{1/2}$, where the distinct peaks located at 778.6 and 781.2 eV are indexed to Co^{3+}. In addition, those peaks at 781.2and 797.3 eV typically represent Co^{2+}. The stronger peaks of Co^{3+} signal than Co^{2+} prove the former accounted for major composition. Figure 3d displays S 2p spectrum and those distinct peaks at 161.4 and 162.5 eV can be in good agreement with S $2p_{3/2}$ and S $2p_{1/2}$, respectively. The peak of binding energy located at 161.4 eV is derived from low coordination near the surface, while the binding energy at 162.5 eV corresponds to metal-sulfur bond (Ni-S and Co-S)[15]. Moreover, the appearance of Ni^{3+} will introduce additional electrons by n-type doping and those Co^{2+} cations will synchronally offer superfluous holes served as p-type doping. Based on the harvest of self-doping, higher conductivity could be achieved, which is beneficial to electrochemical performance (especially in high rate ability) [25]. All above information manifests that the sample of $NiCo_2S_4$ is composed of multiple valence of Ni^{2+}, Ni^{3+}, Co^{2+}, Co^{3+} cations, S^{2-} anions, and these mixed valences provide the possibility of rich redox reactions.

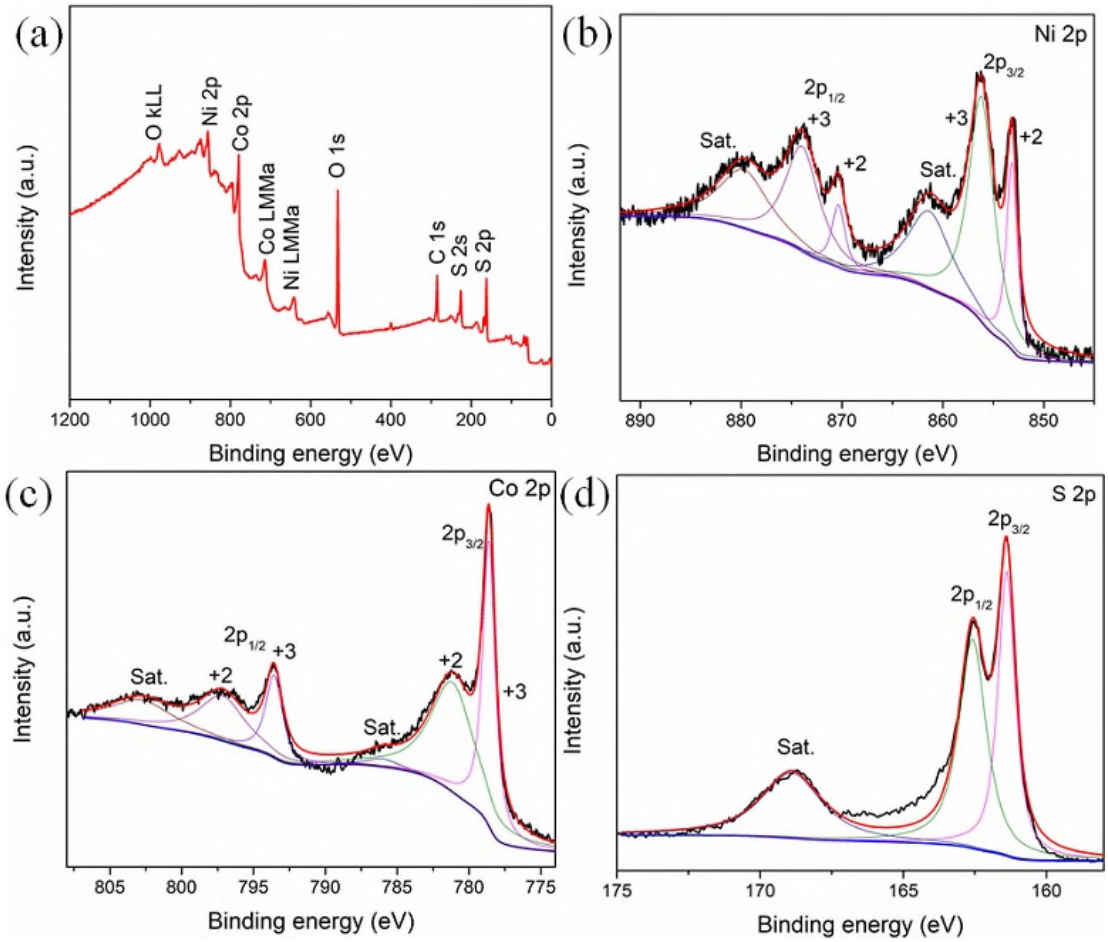

Figure 3 (a) XPS survey spectrum of $NiCo_2S_4$, (b–d) XPS spectra of Ni 2p, Co 2p, and S 2p, respectively.

The porosity has a strong relationship to electrochemical reaction sites and the sample of NCO and $NiCo_2S_4$ was explored by N_2 adsorption/desorption tests at 77 K, and the obtained adsorption/desorption isotherms are presented in figure 4a. These two isotherms of NCO and $NiCo_2S_4$ pertain to Langmuir H4-type with a noticeable hysteresis loop in the range of 0.4 ~ 1 P/P_0 (the latter one distributes in 0.65 ~ 1 P/P_0), which indicates that they hold the characteristic of microporous and mesoporous. The BET specific area of $NiCo_2S_4$ is calculated to be 79.9 $m^2 g^{-1}$, which is inferior to NCO matrix (99.6 $m^2 g^{-1}$) because of the new large nanoparticles, but it is still much larger than most other $NiCo_2S_4$ reported values, for example, ZIF-$NiCo_2S_4$ (50.56 $m^2 g^{-1}$)[15], nickel cobalt sulphides (21.3 $m^2 g^{-1}$)[26], C-$NiCo_2S_4$ (64.7 $m^2 g^{-1}$)[27], $NiCo_2S_4$ (24.39 $m^2 g^{-1}$)[28], $NiCo_2S_4$ nanoparticle (42.79 $m^2 g^{-1}$) [29], C-$NiCo_2S_4$ nanoflakes (56.8 $m^2 g^{-1}$)[30] and just less than $NiCo_2S_4$ aerogels (125.7 $m^2 g^{-1}$). In addition, the pore volume of sample of $NiCo_2S_4$ is ca. 0.256 $cm^3 g^{-1}$. In a word, this rough surface provides rich active sites to electrolyte permeation. The pore size distribution (PSD) was calculated by Barrett-Joyner-Halenda (BJH) method, and the results are as shown in Figure 4b. The BJH pore size distribution is extracted from desorption branch and the PSD of NCO is mainly distributed in the zone of less than 10 nm, but $NiCo_2S_4$ mainly distributes 1~3 nm and 10 ~ 30 nm zone. All these results confirmed that NCO and $NiCo_2S_4$ have a typical mesoporous structure. Especially for $NiCo_2S_4$, suitable PSD containing both big and small hole distribution is beneficial to KOH electrolyte infiltration, transfer, and supply rich redox sites [31, 32].

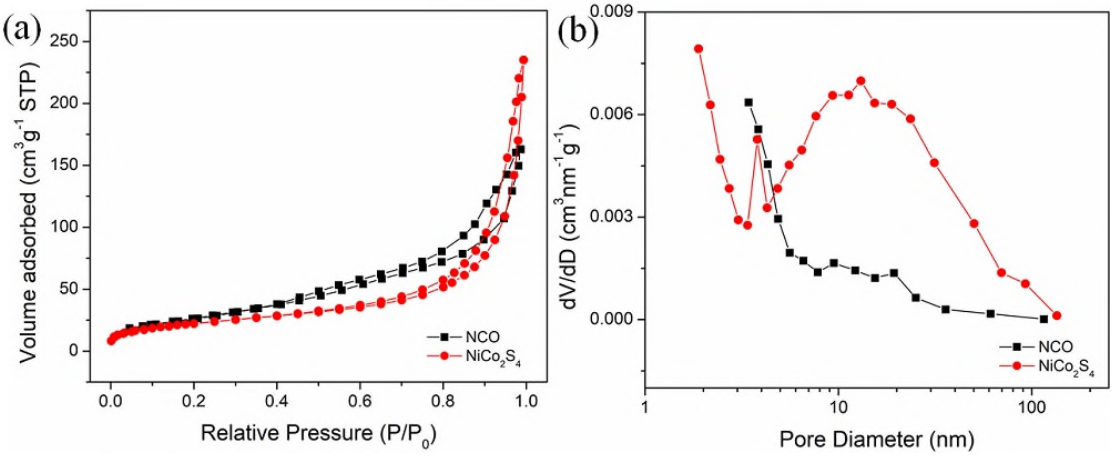

Figure 4 (a) N_2 adsorption/desorption isotherms, (b) BJH pore size distribution.

Electrochemical performance of the synthesized NCO and $NiCo_2S_4$ was firstly evaluated by cyclic voltammetry (CV) measurement in a potential window of 0 ~ 0.6 V. Figure 5a displays the CV curves of $NiCo_2S_4$ at different scanning rates ranging from 2 to 20 mV s^{-1}. With 20 times increase of scan rate, only 0.099 V potential of anodic peak deviates which indicates extremely low polarization. Besides, the profile of CV curves occurs little distortion during the increase, implying that the $NiCo_2S_4$ electrode holds quick response behavior. All these CV curves exhibit a couple of redox reaction meaning typical battery-type behavior, corresponding to convention of Ni^{2+}/Ni^{3+} and $Co^{2+}/Co^{3+}/Co^{4+}$ [15]. Owing to nearby redox potential of Ni/Co cations, only one couple of redox peaks can be observed which is caused by their overlapped peak currents [25]. To further explore the control step of redox reactions, the relationship of scan rate and

anodic current density was fitted and the results are shown in figure 5b. The linear relation of current and the square root of scan rate (Pearson ratio is close to 0.999) indicates that the controlled diffusion is kinetic process [33]. Figure 5c shows the comparison of $NiCo_2S_4$ and NCO CV curves at the same scan rate of 20 mV s^{-1}. It can be noticed that the oxidation (or reduction) peak current of $NiCo_2S_4$ is higher than that of NCO and the closed CV curve area of the former one is much larger, indicating higher capacitance of $NiCo_2S_4$. Figure 5d presents the $NiCo_2S_4$ galvanostatic charge/discharge (GCD) curves which were performed at 1 ~ 20 A g^{-1} (the detailed information of 0 ~ 200 s is shown in Figure S1). Each GCD curve displays excellent symmetry and in apparent IR drop can be observed, which indicates the excellent reversibility and high conductivity.

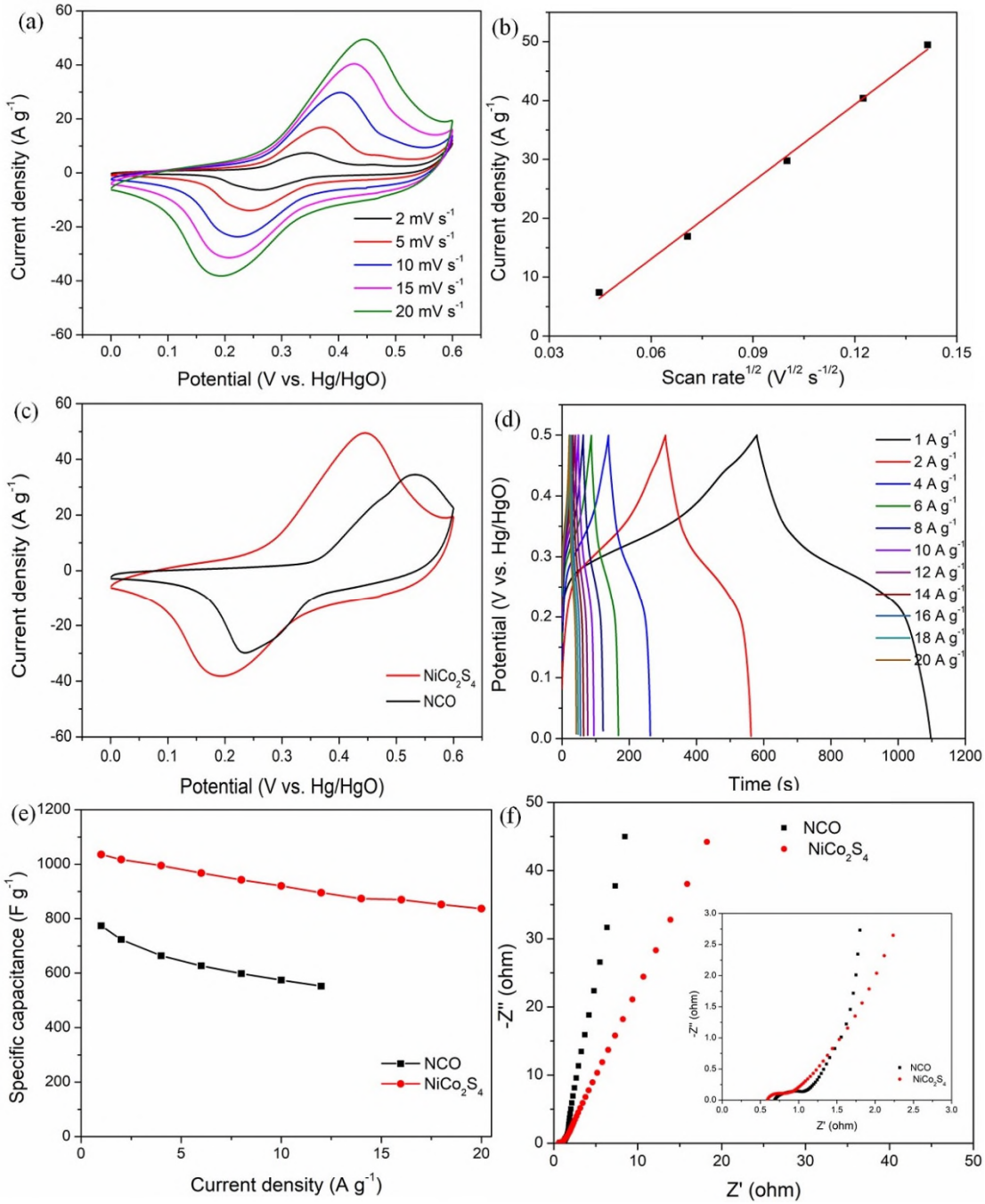

Figure 5 (a) CV curves of $NiCo_2S_4$ at various scan rates, (b) relation of current *vs.* square root of scan rate, (c) CV curves of $NiCo_2S_4$ and NCO at 20 mV s^{-1}, (d) GCD curves of $NiCo_2S_4$ at various current densities, (e) specific capacities of $NiCo_2S_4$ and NCO at various current densities, (f) Nyquist plots of NCO and $NiCo_2S_4$ (inset is enlarged Nyquist plots)

Figure 5e shows the specific capacity of $NiCo_2S_4$ and NCO at different current densities from 1 to 20 A g^{-1}. The high specific capacitance value of $NiCo_2S_4$ (calculated by equation 1) are 1035.1, 967.2, 920.0, 869.7, and 836.4 F g^{-1} at current densities of 1, 6, 10, 16 and 20 A g^{-1}, respectively. Compared with NCO, the specific capacitance of $NiCo_2S_4$ is highly ameliorated. Taking the example of current density at 1 A g^{-1}, the specific capacitance of $NiCo_2S_4$ compares to NCO increase 33.8%. The capacity of $NiCo_2S_4$ has remained 80.8% after the current density has increased twentyfold, showing excellent rate performance. Gratifyingly, it is much higher than other reported values, such as $NiCo_2S_4$ nanoparticles (77%, 10 times)[34], $CoNi_2S_4$-Graphene-2D-$MoSe_2$ (50.8%, 20 times)[35], $NiCo_2S_4$ (65%, 10 times)[36], DNA-$NiCo_2S_4$ (74.3%, 15 times)[37]. The excellent rate performance is honored by the high conductivity and low transfer resistance which benefited by sheet structure during the redox reaction. The resistance properties of the $NiCo_2S_4$ and NCO were measured by electrochemical impedance spectroscopy (EIS), which was conducted in the frequency region from 10^{-2} Hz to 10^5 Hz with a 5 mV AC perturbation (as shown in Figure 5f). Both the two EIS spectra are composed of two regions, one straight line that implies Warburg resistance in low frequency and the semicircle stands for charge transfer resistance in high frequency. According to the fitting of equivalent circuit (as shown in Figure S2), $NiCo_2S_4$ holds smaller internal resistance of 0.61 Ω than NCO (0.68 Ω) verifying the high conductivity of the former one. On the other side, charge transfer resistance of $NiCo_2S_4$ (0.22 Ω) is also smaller than NCO (0.55 Ω). Overall, the small resistance and well electron/ions transport of $NiCo_2S_4$ can be attributed to porous hierarchical structure which facilitates OH^- cations fast transfer, and it's favorable to electrochemical rate performance.

To fully assess the practical potential of the synthesized $NiCo_2S_4$ for high rate energy storage devices, an asymmetric supercapacitor (ASC) was assembled, using $NiCo_2S_4$ as positive electrode and AC as negative one (as shown in Figure 6a). Figure S3 displays the CV curves of $NiCo_2S_4$ and activated carbon electrodes in potential windows of -1.0 ~ 0 and 0 ~ 0.6 V at the scan rate of 20 mV s^{-1} in traditional three-electrode system, respectively. These results indicate that both two electrodes could be assembled in a device whose operation potential window can extend to as high as 1.6 V. Figure 6b shows a series of ASC CV curves in 0 ~ 1.6 V with different scan rates from 5 to 50 mV s^{-1}. The profile of these curves appears distinct rectangular-quasi features, confirming their dual contribution of activated carbon (EDLC performance) and $NiCo_2S_4$ (battery-type performance). Meanwhile, GCD tests were also conducted in 0 ~ 1.6 V at various current densities ranging from 0.5 to 10 A g^{-1} (Figure 6c). The symmetric profile and low IR drop manifest desirable electrochemical performance in potential.

Moreover, the specific capacity of the ASC was calculated by CV and GCD, respectively, and the results are presented in Figure 6d. The maximum specific capacitance by GCD calculation is 99.7 F g^{-1} at 0.5 A g^{-1} and it holds at 65.6 F g^{-1} after the current increases to 10 A g^{-1}. The specific capacitance by CV is calculated to be 102.4, 96.5, 90.1, 86.0, 82.8, 80.5 F g^{-1} at 5, 10, 20, 30, 40, 50 mV s^{-1}, respectively. In general, the device exhibits excellent rate performance of 78.6% after tenfold (scan rate) increase. This favorable rate performance is much superior to most previous reports, for instance, $NiCo_2S_4$ nanosheet//AC (51.4%, 20 fold) [38], $NiCo_2S_4$ aerogel//AC (54.9%, 10 fold)[39]. Due to the excellent cycle performance of NCO and the high specific capacity of $NiCo_2S_4$, it will be interesting to explore whether $NiCo_2S_4$ composite can maintain excellent cycle or not. It can be seen that the cycle durability of the ASC device over 2 000 cycles of GCD tests at a current density of 5 A g^{-1} and the results are shown in figure 6e. The capacity was maintained at 92.4% of the initial capacity after 2 000 cycles, exhibiting outstanding cycle stability.

The energy density and power density are key parameters for supercapacitors in practical applications. Based on the capacitance calculated by GCD, the energy density and power density are obtained (calculated by equation 4 and 5) and the Ragone plots are shown in Figure 6f. Remarkably, the maximum energy density of the ASC is 35.4 Wh kg^{-1} at 0.4 kW kg^{-1}, which is higher than some recently reported values, for example, $NiCo_2S_4$ rGO//AC (27.5 Wh kg^{-1}) [40], rGO/$CoNiS_x$/N–C//AC(32.9 Wh kg^{-1})[41], $Ni_xCo_{3-x}S_4$//carbon xerogels (32.2 Wh kg^{-1})[23]. With the power density increasing up to 8 kW kg^{-1}, it still remains the energy density of 23.3 Wh kg^{-1}. These desirable results reveal that the $NiCo_2S_4$ ASC is capable of high rate energy storage devices.

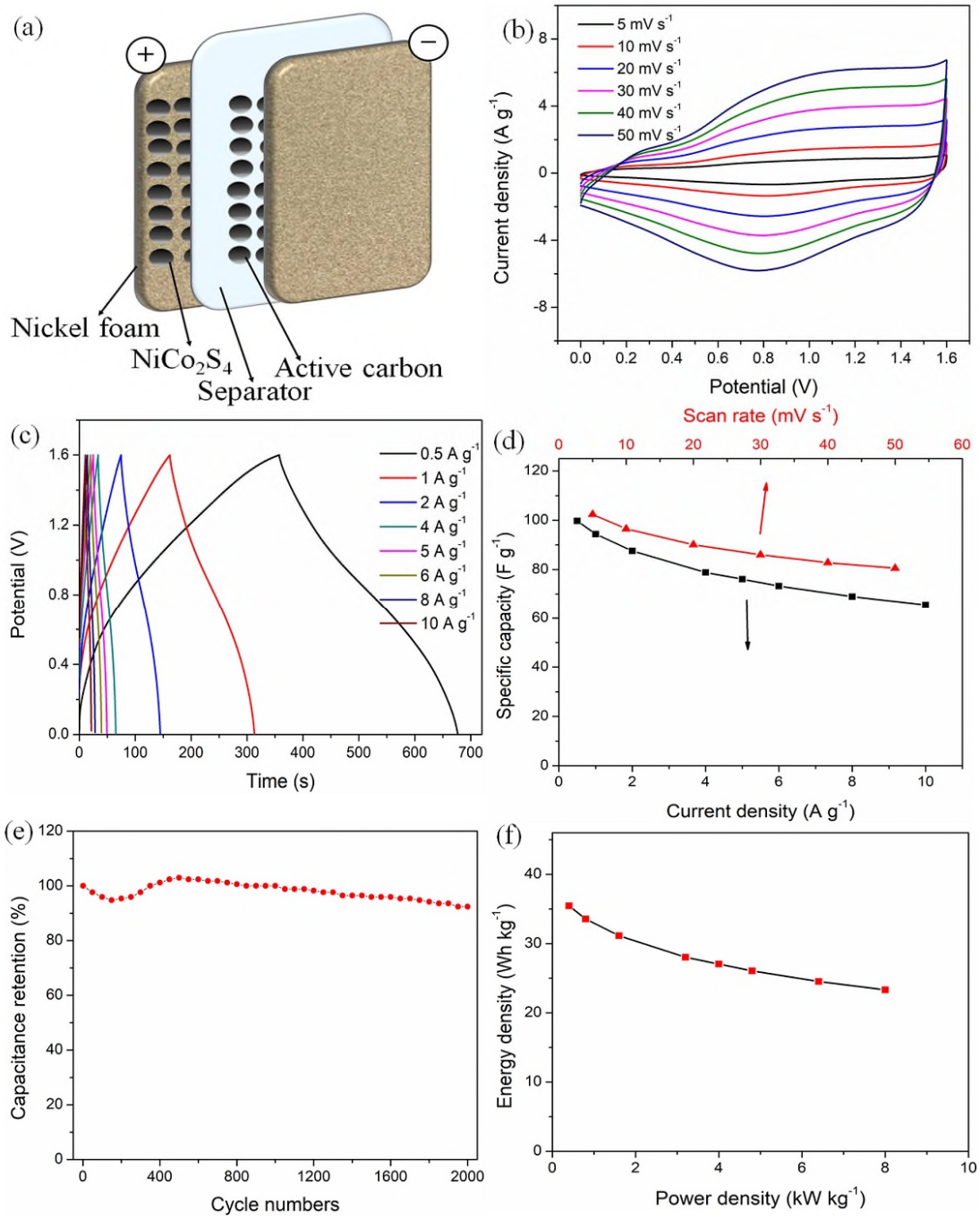

Figure 6 (a) Structural diagram of the $NiCo_2S_4$//AC, (b) CV curves with different scan rates of the ASC, (c) GCD curves with different current densities of the ASC, (d) Specific capacitance of the ASC calculated by various current densities and scan rates, (e) Cycle performance of the ASC at a current density of 5 A g^{-1}, (f) Ragone plots of the ASC energy density *vs.* power density.

The inspiring electrochemical performance of $NiCo_2S_4$ could be ascribed to the following reasons. The sheet structure can buffer the volume variation to increase cycle performance. In addition, the original NCO acts as backbone substrate role for constructing $NiCo_2S_4$ nanoparticles, which is beneficial to shorten OH^- transportation pathway and diminish transfer resistance of the electrode, contributing to high rate performance. The rough surface, porous structure and high specific area features could

provide $NiCo_2S_4$ more exposed to electrochemical active sites to fully embrace KOH electrolyte. The capacity can be largely enhanced by the synergistic effect of multiply valence of nickel and cobalt cations. Besides, the wonderful performance of ASC device could be attributed to the special bridge of high capacity $NiCo_2S_4$ nanoparticles on high cycle stability NCO nanosheet.

4. Conclusion

In summary, the porous hierarchical $NiCo_2S_4$ was successfully synthesized using the synthesized NCO nanosheets as chemical template by a hydrothermal process. The structured NCO nanosheets firstly act as a backbone and eventually converts to $NiCo_2S_4$ by sulfidation. Owing to high porosity (79.9 $m^2 g^{-1}$), hierarchical structure, suitable pore size, mixed cobalt and nickel valence, superior electrochemical performance in supercapacitor of $NiCo_2S_4$ electrode materials is achieved, especially in rate performance (80.9% retention of 20 times increase). In addition, the assembled asymmetric supercapacitor ($NiCo_2S_4$//AC) can deliver a maximum energy density of 35.4 Wh kg^{-1} at 0.4 kW kg^{-1} and excellent rate performance. Overall, this synthesized routine provides a new strategy to construct inspiring hierarchical $NiCo_2S_4$ electrode materials, which could be served as a promising alternative way for high rate performance energy storage devices.

5. Acknowledgments

This work was financially supported by the National Natural Science Foundation of China (Nos. 51202150 and 51272161), Shenzhen Basic Research Program (Nos. JCYJ20170817102025753, JCYJ20170818100134570), China Postdoctoral Science Foundation (No. 2018M633126).

References

[1] M.R. Lukatskaya, B. Dunn, Y. Gogotsi, Multidimensional materials and device architectures for future hybrid energy storage, Nat Commun 7 (2016) 12647.
[2] A. González, E. Goikolea, J.A. Barrena, R. Mysyk, Review on supercapacitors: Technologies and materials, Renewable and Sustainable Energy Reviews 58 (2016) 1189-1206.
[3] Y. Zhang, L. Li, H. Su, W. Huang, X. Dong, Binary metal oxide: advanced energy storage materials in supercapacitors, Journal of Materials Chemistry A 3 (2015) 43-59.
[4] M. Yang, H. Cheng, Y. Gu, Z. Sun, J. Hu, L. Cao, F. Lv, M. Li, W. Wang, Z. Wang, S. Wu, H. Liu, Z. Lu, Facile electrodeposition of 3D concentration-gradient Ni-Co hydroxide nanostructures on nickel foam as high performance electrodes for asymmetric supercapacitors, Nano Research 8 (2015) 2744-2754.
[5] J. Balamurugan, T.T. Nguyen, V. Aravindan, N.H. Kim, J.H. Lee, Flexible Solid-State Asymmetric Supercapacitors Based on Nitrogen-Doped Graphene Encapsulated Ternary Metal-Nitrides with Ultralong Cycle Life, Advanced Functional Materials 28 (2018).
[6] J. Wu, X. Shi, W. Song, H. Ren, C. Tan, S. Tang, X. Meng, Hierarchically porous hexagonal microsheets constructed by well-interwoven MCo 2 S 4 (M = Ni, Fe, Zn)

nanotube networks via two-step anion-exchange for high-performance asymmetric supercapacitors, Nano Energy 45 (2018) 439-447.
[7] H. Chen, J. Jiang, L. Zhang, H. Wan, T. Qi, D. Xia, Highly conductive NiCo(2)S(4) urchin-like nanostructures for high-rate pseudocapacitors, Nanoscale 5 (2013) 8879-8883.
[8] W. Liu, J. Zhang, Z. Bai, G. Jiang, M. Li, K. Feng, L. Yang, Y. Ding, T. Yu, Z. Chen, A. Yu, Controllable Urchin-Like NiCo2S4 Microsphere Synergized with Sulfur-Doped Graphene as Bifunctional Catalyst for Superior Rechargeable Zn-Air Battery, Advanced Functional Materials 28 (2018) 1706675.
[9] Z. Wu, X. Pu, X. Ji, Y. Zhu, M. Jing, Q. Chen, F. Jiao, High Energy Density Asymmetric Supercapacitors From Mesoporous NiCo2S4 Nanosheets, Electrochimica Acta 174 (2015) 238-245.
[10] X. Yu, M. Wang, A. Gagnoud, Y. Fautrelle, Z. Ren, X. Li, Formation of highly porous NiCo 2 S 4 discs with enhanced pseudocapacitive properties through sequential ion-exchange, Materials & Design 145 (2018) 135-143.
[11] Y.P. Gao, K.J. Huang, NiCo2 S4 Materials for Supercapacitor Applications, Chem Asian J 12 (2017) 1969-1984.
[12] N. Wang, Y. Wang, S. Cui, H. Hou, L. Mi, W. Chen, A Hollow Tube-on-Tube Architecture of Carbon-Tube-Supported Nickel Cobalt Sulfide Nanotubes for Advanced Supercapacitors, ChemNanoMat 3 (2017) 269-276.
[13] L. Mei, T. Yang, C. Xu, M. Zhang, L. Chen, Q. Li, T. Wang, Hierarchical mushroom-like CoNi2S4 arrays as a novel electrode material for supercapacitors, Nano Energy 3 (2014) 36-45.
[14] X.-X. Li, X.-T. Wang, K. Xiao, T. Ouyang, N. Li, Z.-Q. Liu, In situ formation of consubstantial NiCo2S4 nanorod arrays toward self-standing electrode for high activity supercapacitors and overall water splitting, Journal of Power Sources 402 (2018) 116-123.
[15] Y. Liu, Z. Wang, Y. Zhong, M. Tade, W. Zhou, Z. Shao, Molecular Design of Mesoporous NiCo2O4 and NiCo2S4 with Sub-Micrometer-Polyhedron Architectures for Efficient Pseudocapacitive Energy Storage, Advanced Functional Materials 27 (2017) 1701229.
[16] X. He, Q. Liu, J. Liu, R. Li, H. Zhang, R. Chen, J. Wang, High-performance all-solid-state asymmetrical supercapacitors based on petal-like NiCo 2 S 4 /Polyaniline nanosheets, Chemical Engineering Journal 325 (2017) 134-143.
[17] R. Li, S. Wang, Z. Huang, F. Lu, T. He, NiCo 2 S 4 @Co(OH) 2 core-shell nanotube arrays in situ grown on Ni foam for high performances asymmetric supercapacitors, Journal of Power Sources 312 (2016) 156-164.
[18] L. Shen, Q. Che, H. Li, X. Zhang, Mesoporous NiCo2O4Nanowire Arrays Grown on Carbon Textiles as Binder-Free Flexible Electrodes for Energy Storage, Advanced Functional Materials 24 (2014) 2630-2637.
[19] P. Wen, M. Fan, D. Yang, Y. Wang, H. Cheng, J. Wang, An asymmetric supercapacitor with ultrahigh energy density based on nickle cobalt sulfide nanocluster anchoring multi-wall carbon nanotubes hybrid, Journal of Power Sources 320 (2016) 28-36.

[20] X. Yang, H. Niu, H. Jiang, Z. Sun, Q. Wang, F. Qu, One-Step Synthesis of NiCo2S4 /Graphene Composite for Asymmetric Supercapacitors with Superior Performances, ChemElectroChem 5 (2018) 1576-1585.
[21] W.H. Fenglin Zhao, Dengmei Zhou, Chemical bath deposition synthesis of nickel cobalt oxides sulfides for high-performance supercapacitors electrode materials, Journal of Alloys and Compounds 755 (2018) 15-23.
[22] F. Yang, Z. Fang, K. Xu, J. Yang, J. Hu, NixCo3−xS4@NiCo2O4 hybrid composites as supercapacitors electrode material, Materials Letters 191 (2017) 101-104.
[23] G.T. Liujun Cao, Jun Mei, Hao Liu, Construct hierarchical electrode with NixCo3-xS4 nanosheet coated on NiCo2O4 nanowire arrays grown on carbon fiber paper for high-performance asymmetric supercapacitors, Journal of Power Sources 359 (2017) 262-269.
[24] S. Raj, S.K. Srivastava, P. Kar, P. Roy, Three-dimensional NiCo2O4/NiCo2S4 hybrid nanostructure on Ni-foam as a high-performance supercapacitor electrode, RSC Advances 6 (2016) 95760-95767.
[25] R.B. Linrui Hou, Muhammad Rehan, Liuniu Tong, Gang Pang, Xiaogang Zhang, Changzhou Yuan, Uniform Hollow Mesoporous Nickel Cobalt Sulfide Microdumbbells_ A Competitive Electrode with Exceptional Gravimetric_Volumetric Pseudocapacitance for High-Energy-Density Hybrid Superapacitors Advanced Electronic Materials 3 (2017) 1600322.
[26] J.J. Haichao Chen, Yuandong Zhao, Li Zhang, Danqing Guo, Dandan Xia, One-pot synthesis of porous nickel cobalt sulphides tuning the composition for superior pseudocapacitance, Journal of Materials Chemistry A 3 (2015) 428-437.
[27] Q.L. Tian Wang, Guodong Zhang, Shijin Zhu, Bo Guan, Junming Zhang, Shuangxi Xing, Yuxin Zhang, Facile preparation and sulfidation analysis for activated multiporous carbon@NiCo2S4 nanostructure with enhanced supercapacitive properties, Electrochimica Acta (2016) 627–635.
[28] G. Sheng, J. Chen, Y. Li, H. Ye, Z. Hu, X.Z. Fu, R. Sun, W. Huang, C.P. Wong, Flowerlike NiCo2S4 Hollow Sub-Microspheres with Mesoporous Nanoshells Support Pd Nanoparticles for Enhanced Hydrogen Evolution Reaction Electrocatalysis in Both Acidic and Alkaline Conditions, ACS Appl Mater Interfaces 10 (2018) 22248-22256.
[29] Y. Zhu, Z. Wu, M. Jing, X. Yang, W. Song, X. Ji, Mesoporous NiCo 2 S 4 nanoparticles as high-performance electrode materials for supercapacitors, Journal of Power Sources 273 (2015) 584-590.
[30] S.G. Mohamed, I. Hussain, J.J. Shim, One-step synthesis of hollow C-NiCo2S4 nanostructures for high-performance supercapacitor electrodes, Nanoscale 10 (2018) 6620-6628.
[31] X. Li, Q. Li, Y. Wu, M. Rui, H. Zeng, Two-Dimensional, Porous Nickel-Cobalt Sulfide for High-Performance Asymmetric Supercapacitors, ACS Appl Mater Interfaces 7 (2015) 19316-19323.
[32] J.L.D.Z. Wei Li, Mesoporous materials for energy conversion and storage devices, Nature Reviews Materials 1 (2016) 1-17.
[33] B.Y. Guan, L. Yu, X. Wang, S. Song, X.W. Lou, Formation of Onion-Like NiCo2 S4 Particles via Sequential Ion-Exchange for Hybrid Supercapacitors, Adv Mater 29

(2017).
[34] X. Ning, F. Li, Y. Zhou, Y.-E. Miao, C. Wei, T. Liu, Confined growth of uniformly dispersed NiCo 2 S 4 nanoparticles on nitrogen-doped carbon nanofibers for high-performance asymmetric supercapacitors, Chemical Engineering Journal 328 (2017) 599-608.
[35] J. Shen, J. Wu, L. Pei, M.-T.F. Rodrigues, Z. Zhang, F. Zhang, X. Zhang, P.M. Ajayan, M. Ye, CoNi2S4-Graphene-2D-MoSe2as an Advanced Electrode Material for Supercapacitors, Advanced Energy Materials 6 (2016) 1600341.
[36] X. Xiong, G. Waller, D. Ding, D. Chen, B. Rainwater, B. Zhao, Z. Wang, M. Liu, Controlled synthesis of NiCo 2 S 4 nanostructured arrays on carbon fiber paper for high-performance pseudocapacitors, Nano Energy 16 (2015) 71-80.
[37] H. Liu, Y. Wang, Z. Li, Z. Yao, J. Lin, Y. Sun, Z. Li, DNA-assisted synthesis of nickel cobalt sulfide nanosheets as high-performance battery-type electrode materials, J Colloid Interface Sci 528 (2018) 100-108.
[38] F. Wang, G. Li, J. Zheng, J. Ma, C. Yang, Q. Wang, Microwave synthesis of three-dimensional nickel cobalt sulfide nanosheets grown on nickel foam for high-performance asymmetric supercapacitors, J Colloid Interface Sci 516 (2018) 48-56.
[39] Q. Gao, X. Wang, Z. Shi, Z. Ye, W. Wang, N. Zhang, Z. Hong, M. Zhi, Synthesis of porous NiCo 2 S 4 aerogel for supercapacitor electrode and oxygen evolution reaction electrocatalyst, Chemical Engineering Journal 331 (2018) 185-193.
[40] Y. Zheng, X. Wang, W. Zhao, X. Cao, J. Liu, Phytic acid-assisted synthesis of ultrafine NiCo 2 S 4 nanoparticles immobilized on reduced graphene oxide as high-performance electrode for hybrid supercapacitors, Chemical Engineering Journal 333 (2018) 603-612.
[41] Q. Chen, J. Miao, L. Quan, D. Cai, H. Zhan, Bimetallic CoNiSx nanocrystallites embedded in nitrogen-doped carbon anchored on reduced graphene oxide for high-performance supercapacitors, Nanoscale 10 (2018) 4051-4060.

Construction of porous hierarchical NiCo2S4 toward high rate performance supercapa

Zhao, Fenglin

2019-11-11

Zhao F, Huang W, Sial MAZG, et al., (2019) Construction of porous hierarchical NiCo2S4 toward high rate performance supercapacitor. Journal of Materials Science: Materials in Electronics, December 2019, Volume 30, Issue 24, pp. 21229–21239

https://doi.org/10.1007/s10854-019-02496-2